High transmission efficiency collection system for laser-accelerated proton beams based on permanent magnet quadrupoles prefocusing

Yang Yan,[1,2] Hao Cheng,[1,2] Yuze Li,[1,2] Yanlv Fang,[1,2] Yadong Xia,[1,2] Qiangyou He,[1,2] Chentong Li,[1,2] Fangnan Li,[1,2] Zhen Guo,[1,2] Yiting Yan,[1,2] Mingfeng Huang,[1,2] Minjian Wu,[1,2] Kedong Wang,[1,2] Kun Zhu,[1,2,3] Xueqing Yan,[1,2,3] and Chen Lin[1,2,3,*]

[1]*State Key Laboratory of Nuclear Physics and Technology, and Key Laboratory of HEDP of the Ministry of Education, CAPT, Peking University, Beijing 100871, China*

[2]*Beijing Laser Acceleration Innovation Center, Huairou, Beijing 101400, China*

[3]*Institute of Guangdong Laser Plasma Technology, Baiyun, Guangzhou 510540, China*

(Received 21 September 2023; accepted 10 April 2024; published 3 May 2024)

A new high transmission efficiency, easily tunable, and cost-effective beam collection system is proposed for laser-accelerated proton beams with large divergence angles and wide energy spectra. In previous experiments conducted at the compact laser plasma accelerator platform of Peking University, a beamline was initially constructed with a collection system based on an electromagnetic quadrupoles (EMQs) triplet. However, due to the limited acceptance angle, the EMQs exhibited a monoenergetic transmission efficiency of only 10% to 20% for laser accelerated proton beams. Permanent magnet quadrupoles (PMQs), known for their high magnetic field gradients, compact size, and lower expenses, are well suited for integration with other readily adjustable transmission elements like EMQs and solenoids, effectively enhancing the beam collection capabilities of the system. In this paper, we show that by introducing a pair of centimeter-sized PMQs in front of the EMQs for beam prefocusing, the beam's transverse size is quickly compressed, enabling transmission of highly divergent protons. Experimental results demonstrate that the prefocusing by PMQs increased the system's transmission efficiency by a factor of 2.44 to 6.01 compared to the original setup, while also enhancing the energy selection based on stronger chromatic effect. This method can be extended to 100 MeV high-energy proton beamlines and is crucial for applications of laser plasma accelerators.

DOI: 10.1103/PhysRevAccelBeams.27.052801

I. INTRODUCTION

Laser plasma acceleration (LPA) has emerged as a powerful contender for future accelerators [1–3] and compact radiation sources [4], owing to its acceleration gradient exceeding that of traditional accelerators by three orders of magnitude [5]. It harnesses the interaction between ultraintense lasers and target materials, driving the collective motion of a large number of electrons within the target to generate an extremely strong longitudinal electric field, capable of accelerating proton beams up to near 100 MeV (currently) within micrometer distances [2]. LPA proton beams offer unique qualities, like low emittance ($\sim 10^{-3}$ mm mrad) [6–8] and high current (10^{13} protons within picoseconds) [9], making them valuable in diverse fields, such as cancer treatment [10–13], materials science [14–16], imaging [17], and high-energy physics [18]. Generally, these applications require proton beams containing large numbers of particles and with specific energies. However, the high gradient and transient nature of laser acceleration make it highly susceptible to nonlinearity and instability. Therefore, LPA proton beams typically have exponentially decaying energy spectra (100%) and large divergence angles (hundreds of mrad). Capturing, transporting, and focusing these proton beams pose the most significant challenges.

The mainstream transmission elements include permanent magnet quadrupoles (PMQs), electromagnetic quadrupole (EMQs), and solenoids. PMQs offer advantages such as high magnetic field gradients of order of 100 T/m, compact size, vacuum compatibility, and cost-effectiveness. Nonetheless, their fixed magnetic field makes the energy adjustment process complex and limits the range [19–22]. EMQs offer adjustable electromagnetic field through current control but have larger sizes and weaker focusing capabilities [23]. Pulsed or superconducting solenoids provide axial symmetry focusing and larger collection angles but require complex

*lc0812@pku.edu.cn

power or cooling systems, making them expensive and challenging to overcome high repetition rate limitations [24–26]. Currently, several beamlines based on the above elements and their performance have been reported. For instance, the extreme light infrastructure beamlines, using a set of PMQs in the collection section, achieves a 15% transmission efficiency for proton beams with an initial half-divergence angle of 87 mrad [27,28]. The beamline of GSI Helmholtz Center, based on two pulsed solenoids, achieves up to 37% transmission efficiency for proton beams with an initial divergence angle of approximately 170 mrad [29,30]. The CLAPA-T high-energy achromatic beamline is designed to use three superconducting solenoids for collection, with a target collection angle of 50 mrad [31]. However, because of the inherent limitations of each transmission element category, these beamlines constructed solely with a single type of collection element find it challenging to simultaneously achieve high transmission efficiency, strong energy adjustment capabilities, and low cost.

A compact laser plasma accelerator (CLAPA) with EMQs triple as the beamline collection section has been built at Peking University [32,33]. The EMQs triple provides excellent stability and adjustability. However, its transmission efficiency is only 10%–20%, due to limitations in the magnet's focusing power, aperture size, and spatial volume. A significant amount of high divergence angle protons are unable to enter the beamline or strike the beamline walls, leading to losses. Considering that PMQs offer strong focusing ability within a compact structure, an increased transmission efficiency collection system scheme with strong tunability and affordability has been theoretically proposed [34], which utilizes PMQs closer to the target for precollection, promptly constraining the beam divergence, and achieves the final focusing in combination with the existing EMQs triple. By synchronously changing the positions of PMQs and currents of EMQs, the centrally transmitted energy of the system can be easily adjusted.

In this paper, we present an experimental study of the high transmission efficiency of collection system, a significant enhancement in the beam density and charge with the addition of PMQs for prefocusing in the system compared to the case with only EMQs triple was observed. Furthermore, the combination of PMQs and solenoids for the CLAPA-T 100 MeV high-energy medical beamline is also discussed, demonstrating the widespread applicability of the PMQs prefocusing scheme.

II. EXPERIMENTAL SETUP

The experiments were conducted on the CLAPA platform at Peking University. Its main design features are presented in Fig. 1. The proton beam generated by laser-target interaction was emitted along the z direction and focused by the collection system consisting of PMQs and EMQs (PMQ1, EMQ1, and EMQ3 for x direction focusing, PMQ2 and EMQ2 for y direction focusing). Radiochromic films (RCFs) or scintillators in the focus detection plane were used to observe the particle collection status, and a 45° bending magnet was used to further energy and emittance analysis of the focused beam. A detailed description of the experimental setup and methods is provided below.

A. Proton source

A p-polarized laser pulse with energy $E_L = 1.3$ J and duration $\tau = 30$ fs was focused into a spot with a full width at half maximum diameter of 5 μm (with 25% of the total energy, corresponding to an intensity of 5.5×10^{19} W/cm^2) and was incident onto a 7 μm thick aluminum target with an incident angle of 30° to the target normal direction. The accelerated protons were detected with calibrated RCF stacks [35]. Due to protons depositing the most energy at the Bragg peak, RCF can be utilized to detect a monoenergetic proton beam whose Bragg peak aligns with the active layer. The RCF stacks in the experiment were composed of either two pieces of HD-V2 RCFs covered with 10 μm aluminum foil or one piece of HD-V2 RCF covered with 55 μm aluminum foil, allowing for detection of 1.0, 2.5, and 3.1 MeV protons according to the Monte Carlo program SRIM [36] simulation results. The particle number spectrum dN/dE per unit energy is assumed to satisfy the exponentially decreasing

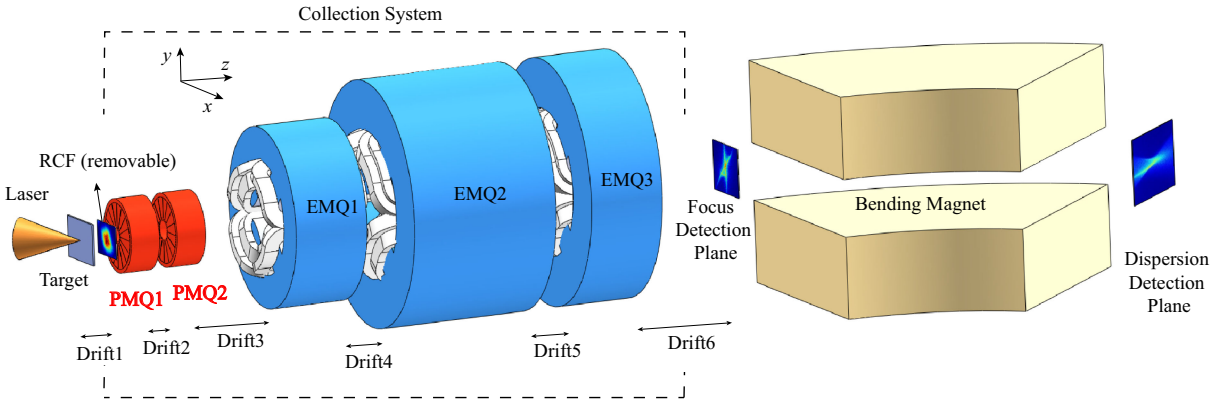

FIG. 1. Experimental setup at CLAPA.

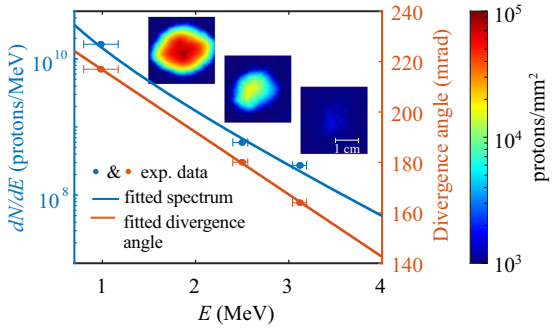

FIG. 2. Proton energy spectrum and divergence angle measured by RCF stacks located 40 mm behind the target, along with the corresponding fitted curves.

distribution $\frac{dN}{dE} = \frac{N_0}{E}\exp\left(-\frac{E}{k_B T}\right)$ [37,38], and the divergence angle $\theta = a \cdot E + b$ follows a linearly decreasing distribution [39,40]. By fitting the three data points measured by RCFs ($N_0 = 2.3 \times 10^{10}$, $k_B T = 0.8$ MeV, $a = -22.7$ and $b = 223.4$), the proton energy spectrum and divergence angle were obtained, as shown in Fig. 2.

B. Magnet parameters determination, characterization, and simulation verification

Key parameters that determine the collection capability and focusing energy of the collection system primarily include the hardware specifications of PMQs (radii, lengths, and magnetic field gradients) and adjustable parameters of the drift regions' lengths (l_{drift1}, l_{drift2}, and l_{drift3}) as well as the magnetic field gradients of EMQs. Taking into account the laser shooting results, our objective is to maximize the transmission efficiency η of MeV-level energy protons. Here, η is defined as the ratio of the number of protons within the focal spot (with a distance from the center of the beam spot less than ± 10 mm) and having the designated energy to the initial number of protons with that energy. In the first step, we assumed hard-edge models for the magnetic fields and, with constraints, such as maximum magnetic field strengths, magnet volumes, and magnetic attraction forces [28], we introduced a genetic optimization algorithm for preliminary parameters determination [34].

According to the design parameters, two PMQs were fabricated. We used a Halbach structure, where each PMQ was assembled from 16 neodymium iron boride magnetic poles. To prevent demagnetization of the permanent magnetic material due to beam irradiation, 10 mm thick stainless steel plates were installed at the front and rear of the PMQs for shielding, and 4 mm thick shielding pipes were installed inside the PMQs' inner apertures, effectively blocking the passage of MeV protons. In addition, in order to avoid the temperature increase of the shielding pipes caused by long-term dose deposition and affecting the magnetic field of PMQs, based on the calculation considering the specific heat of the material, the number of consecutive shooting shots needs to be controlled within tens of thousands [28]. We conducted magnetic field measurements using the Hall probe, and the obtained longitudinal and transverse magnetic field distributions are shown in Figs. 3(a) and 3(b), respectively. These real magnetic field data were incorporated into the optimization algorithm for fine-tuning the adjustable parameters, and the final parameter set was determined. For instance, when the target proton energy for collection is set to 3.5 MeV, the corresponding optimal parameter set is listed in Table I, where $R_{\text{linear field}}$ represents the radius of the region where the magnetic field exhibits an linear distribution, covering approximately 60% of the bore of the PMQs. The parameter values highlighted in bold in this table are tailored to the 3.5 MeV proton specifications, while the remaining values are fixed parameters.

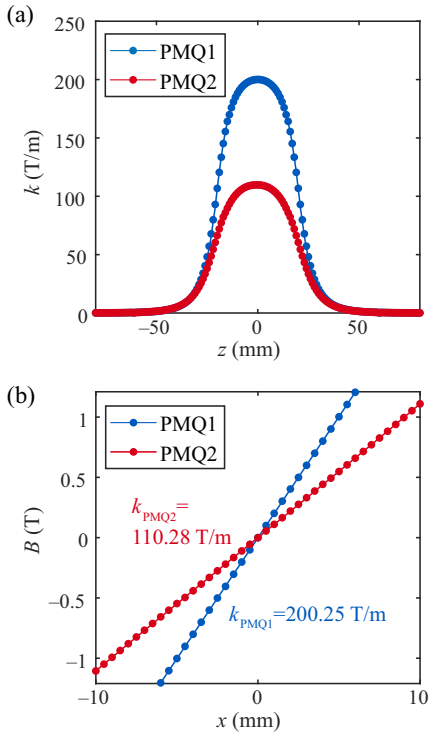

FIG. 3. Measured distribution of magnetic field strength B or magnetic field gradient $k = \partial B/\partial r$ along the (a) longitudinal and (b) transverse directions.

These parameters were then input into the beam transport simulation program TRACK, with an initial divergence angle of 150 mrad and an energy spread of $\pm 5\%$ for the proton beam. The resulting beam envelope and beam spot at the focal point from the combination of PMQs and EMQs focusing is illustrated in Fig. 4(b). For comparison, Fig. 4(a) presents the beam transport scenario with only EMQs focusing. The star-shaped beam profiles are due to the combined effects of chromaticity effect and the nonlinear fringe magnetic fields of the magnet [19,41]. In the case of EMQs triplet, a notable proportion of protons have diverged excessively after traveling through the drift section and are lost at the entrance and on the walls of EMQ1. Coupled with

TABLE I. Key parameters of the enhanced collection system with 3.5 MeV central transmission energy.

Element	Length (mm)	$R_{\text{linear field}}$ (mm)	Field gradient (T/m)
Drift1	**37.4**		
PMQ1	40	6	200.25
Drift2	**27.4**		
PMQ2	40	10	110.28
Drift3	**135.2**		
EMQ1	100	12	**17.33**
Drift4	59		
EMQ2	200	28	**17.17**
Drift5	52		
EMQ3	100	28	**12.51**
Drift6	2355		

the losses stemming from the asymmetrical focusing of the quadrupole lens, only 16.1% of the protons can be effectively transmitted through the EMQs triplet. The integration of PMQs reduces the initial drift region length, effectively suppresses beam divergence using their strong focusing capability, and significantly enlarges the acceptance angle of the system. Although there is still some beam lost on the walls of PMQs due to the quadrupole lenses' asymmetric focusing, the system's transmission efficiency has been elevated to 64.6%, approximately 4 times that of the EMQs-only system.

C. Experimental methods and mover system

The precise control of PMQs' positions is a crucial aspect of the experiment, so we have designed a magnet displacement system. As shown in Fig. 5(a), the PMQs are equipped with carriages, guides, and vacuum motors. These components allow for adjusting the relative distances between magnets and tuning the system to transfer various energies.

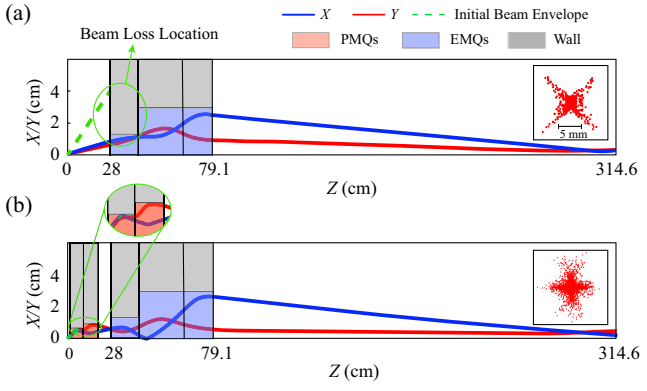

FIG. 4. Beam envelope and focused beam spot (the inset on the right) simulated by the TRACK software, showing the focusing of EMQs triplet only (a) and a combination of PMQs and EMQs (b). In both cases, the proton beam features a central energy of 3.5 MeV, an energy spread of ±5%, and an initial divergence angle of 150 mrad.

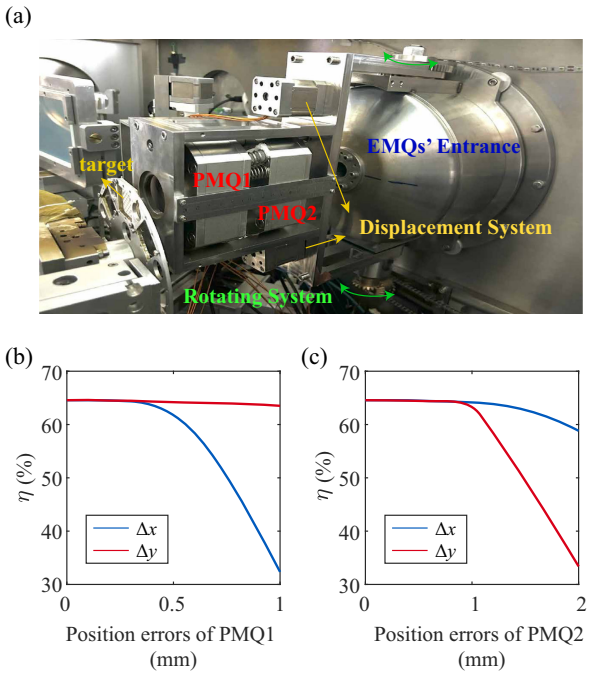

FIG. 5. (a) Physical installation diagram of the PMQs + EMQs beamline collection system. The displacement system controls the longitudinal position of the PMQs, and the rotation system enables the overall movement of the PMQs to switch between different post-target configurations. (b) Position errors for PMQ1 and (c) PMQ2, primarily due to mechanical installation errors, are simulated by adding errors to the beamline parameters centered around 3.5 MeV as shown in Table I.

Additionally, in our setup, PMQ1 is positioned very close to the target, approximately 4 cm away. This proximity could potentially obstruct the operation of other devices located behind the target, such as cameras for observing the focused lasers, RCFs, and imaging plates used for diagnosing the proton source. To address this concern, we have designed the rotating system depicted in Fig. 5(a). It mounts the PMQs and related components on a rotatable support, allowing for their collective movement. This facilitates the convenient alteration of the operational status of the PMQs and other post-target devices and also makes it convenient for conducting comparative experiments with or without PMQ prefocusing.

The error analysis presented in Figs. 5(b) and 5(c) demonstrates that when PMQs exhibit certain lateral positional errors denoted as Δx or Δy, it leads to a decrease in transmission efficiency. Additionally, because PMQ1 provides focusing in the x direction and PMQ2 in the y direction, misalignments in PMQ1's x position and PMQ2's y position have a more pronounced impact. These misalignments may arise from mechanical installation errors of the PMQs but can also occur due to the magnetic center not aligning with the geometric center of the PMQs. To address this, the entire

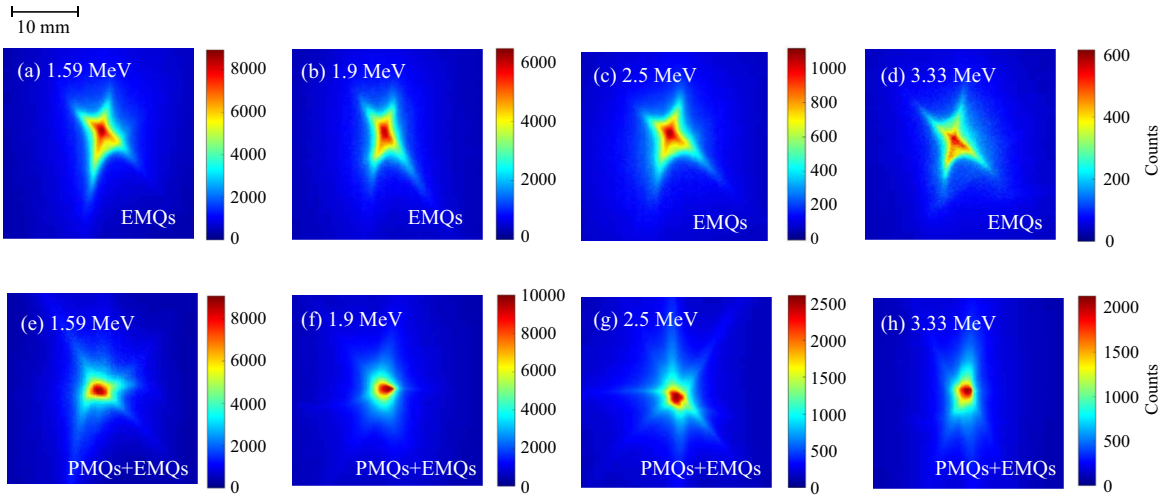

FIG. 6. Experimentally recorded beam profiles with magnets tuned for (a), (e) 1.59 MeV, (b), (f) 1.9 MeV, (c), (g) 2.5 MeV, (d), (h) 3.33 MeV protons with the focusing of an EMQs triplet only (a)–(d) and a combination of PMQs and EMQs (e)–(h). The color scale represents the count from the EMCCD used for detecting the beam spots, which is proportional to beam intensity.

system has undergone precise position calibration using collimated lasers, allowing us to control installation errors to within 0.5 mm. Furthermore, the dipole field component magnitudes [42] measured using the coil rotation method for PMQ1 and PMQ2 are 80 and 17 Gs, respectively. This indicates that the displacement between the magnetic and geometric axes is estimated to be approximately 40 μm and 15 μm [19], respectively, which has negligible effects on transmission efficiency. This implies that the system has met the experimental requirements.

III. EXPERIMENTAL RESULTS

We have conducted the beam transport experiments. The charge density distributions of beam spot were detected by scintillators and are shown in Fig. 6, exhibiting the same star-shaped beam profile as the previous simulation results. Each column corresponds to the beam spot signals at center focusing energies of 1.59, 1.9, 2.5, and 3.33 MeV, respectively. The top row represents results from EMQs triplet focusing and transport alone, while the bottom row represents results from combined PMQs and EMQs focusing. For protons in the energy range of 1.59 to 3.33 MeV, with the assistance of PMQs for focusing, the maximum charge density is increased by a factor of 1.01 to 3.46 compared to focusing with only EMQs.

By quantifying the total charge within each beam spot and comparing it with the measured proton source charge, the system's transmission efficiency η for different proton energy ranges can be obtained, as shown in Fig. 7. The dashed line represents the transmission efficiency obtained from TRACK simulations, where the initial divergence angle variation with energy was considered. The points represent experimental values, which match the simulation results well. The results indicate that the inclusion of PMQs allows for the collection of protons over a larger angular range, resulting in an increase in transmission efficiency by a factor of 2.44 to 6.01.

After the collection system focuses the proton beam, it forms a waist in the horizontal direction (x axis) at the system's image point. This image point also corresponds to the object point of the bending magnet in the x direction. After undergoing energy analysis by the bending magnet, protons of different energies separate along the x direction at the bending magnet's image point. In the vertical direction (y axis), the bending magnet has no impact on protons in linear optics. Due to chromaticity, the protons at the central energy form a waist at the image point of the bending magnet, while the others do not. This results in a butterfly-shaped pattern with a narrow center and gradually widening wings on both sides. On the one hand, monitoring

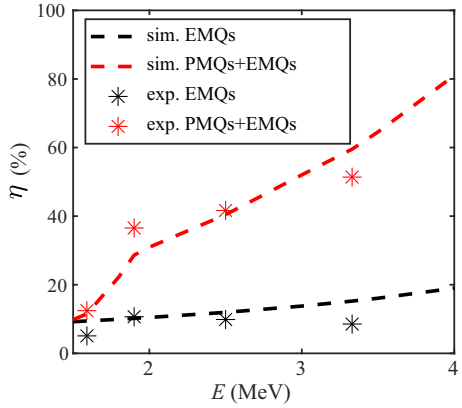

FIG. 7. Simulated (dashed line) and experimental (asterisk) measurements of the transmission efficiency for both EMQs transport only (black) and combined PMQs with EMQs transport (red).

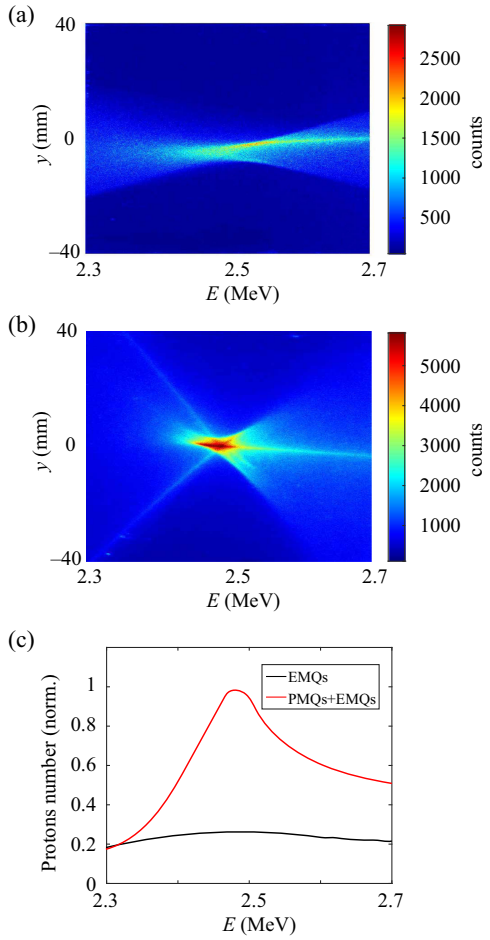

FIG. 8. Proton beam, after passing through (a) EMQs and (b) PMQs + EMQs collection (the central focusing energy here is 2.5 MeV), undergoes energy analysis by the bending magnet, resulting in a butterfly-shaped beam profile. In the x direction, this corresponds to energy information, while in the y direction, it reflects the chromatic dispersion effect. (c) Presents the numbers of protons of each energy in the corresponding beams, which are normalized relative to the maximum value.

the beam's signal postbending magnet offers insights into the energy spread permitted by the collection system, as depicted in Figs. 8(a) and 8(b). With PMQs for prefocusing, two notable effects are observed. First, the beam intensity at the central energy of 2.5 MeV is enhanced by about 4 times, further verifying its collection efficiency improvement effect. Second, the wings of its butterfly-shaped beam profile significantly widen because the difference in amplification factors for protons of different energies increases. Counting the number of protons at various energy levels within the defined focusing range (where the y direction width is within ± 10 mm), as seen in Fig. 8(c), if we consider the range exceeding 90% of the maximum value as the dispersion range, the energy dispersion for the EMQs system is 13.2%, while for the PMQs + EMQs system, it is only 2.0%. This implies that the permanent magnet prefocusing system further enhances its energy selection capability, offering the advantage of more precise control over the specific energy of the transmitted beam in proton beam applications. On the other hand, single-shot emittance measurements based on the bending magnet can be achieved [43,44], as the beam's root-mean-square (rms) size in the y direction $\sigma_{y,n,\mathrm{rms}}(E) = \sqrt{R_{11}(E)^2\sigma_{y0}^2 + (\frac{\varepsilon_{y,n,\mathrm{rms}}}{\beta\sigma_{y0}})^2 R_{12}(E)^2}$, where R_{ij} refers to the element of the transport matrix, σ_{y0} is the beam source size, and $\varepsilon_{y,n,\mathrm{rms}}$ represents the rms emittance in the y direction. Calculations reveal that the normalized rms emittance after passing through EMQs is 0.057 mm mrad, while it increases to 0.084 mm mrad when PMQs are added to the system. This emittance growth can be attributed to both the collection of protons with a wider angular spread and the increased fringe fields generated by the additional PMQs.

IV. CONCLUSION AND OVERLOOK

The aforementioned system parameter design and experiments were tailored for the CLAPA experimental system using a 60 TW laser to generate MeV-level proton beams [45]. We also verified the feasibility of this method for scenarios where higher proton energy needs to be transmitted and the main focusing element is not a quadrupole lens. Take the example of CLAPA-T, a novel proton therapy facility being developed at Peking University. It will utilize a 2 PW laser to yield proton beams in the 100 MeV range. The beamline collection segment of CLAPA-T is devised with three superconducting solenoids to gather and transform the initially divergent proton beam into a quasiparallel beam [31]. As portrayed in the simulation results depicted in Fig. 9, due to the confined magnetic field strength of the solenoids, the collection angle of the solenoids group is about 50 mrad, and a

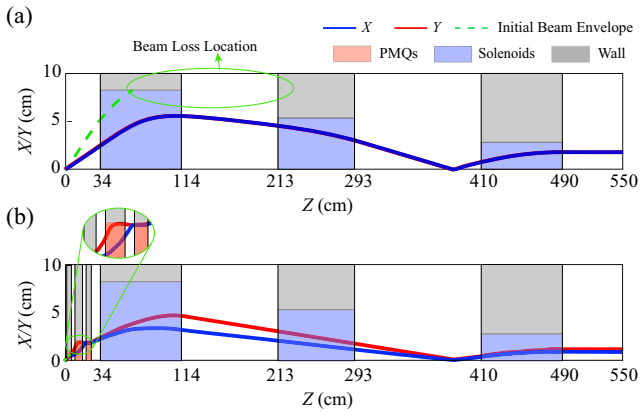

FIG. 9. Solution for enhancing transmission efficiency of the 100 MeV high-energy medical beamline for CLAPA-T. (a) Beam envelope simulation results collected solely by the superconducting solenoid group and (b) by the combined collection of PMQs and the solenoid group. The proton beam has a central energy of 100 MeV, energy dispersion of $\pm 1\%$, and an initial divergence angle of 150 mrad.

notable portion of protons is lost at the wall plane and entrance of the second solenoid. For a proton beam with a 150 mrad initial divergence angle and 100 MeV energy, the corresponding transmission efficiency for this collection section stands at 24%. However, we found that the compact and high-gradient PMQs can also present a solution for augmenting the transmission efficiency of this system. By prefocusing with three PMQs featuring magnetic field gradients of 514, 218, and 100 T/m, along with lengths of 6, 8, and 6 cm, respectively, the system's collection angle can be elevated to 90 mrad, leading to a 2.1-fold enhancement in transmission efficiency. According to Ref. [19], PMQs with these parameters are achievable. In the realm of laser proton therapy, this implies that achieving therapeutic effects could require fewer shots, thereby effectively reducing costs and saving time.

In summary, we presents a scheme for enhancing the transmission efficiency of the laser-accelerated proton beam collection system by implementing PMQs for prefocusing. Based on the system parameter design using genetic algorithms and a reliable magnet mover mechanical system, experiments have confirmed that the prefocused collection system incorporating PMQs successfully increases the particle count and narrows the energy spectrum range in the transmitted beam. The emittance of the focused beam is also discussed. Furthermore, a prospect and simulation for improving the transmission efficiency in the context of 100 MeV high-energy medical beamline is presented. This solution is cost-effective, space-saving, and highly adjustable, offering the potential to further expand the application scenarios of laser-accelerated proton beams.

ACKNOWLEDGMENTS

This work was supported by the National Natural Science Foundation of China (Grants No. 12122501, No. 11975037, No. 61631001, and No. 11921006) and the National Grand Instrument Project (No. 2019YFF01014404).

[1] I. J. Kim, K. H. Pae, I. W. Choi, C.-L. Lee, H. T. Kim, H. Singhal, J. H. Sung, S. K. Lee, H. W. Lee, P. V. Nickles *et al.*, Radiation pressure acceleration of protons to 93 MeV with circularly polarized petawatt laser pulses, Phys. Plasmas, **23**, 070701 (2016).

[2] A. Higginson, R. Gray, M. King, R. Dance, S. Williamson, N. Butler, R. Wilson, R. Capdessus, C. Armstrong, J. Green *et al.*, Near-100 mev protons via a laser-driven transparency-enhanced hybrid acceleration scheme, Nat. Commun. **9**, 724 (2018).

[3] S. Steinke, J. Bin, J. Park, Q. Ji, K. Nakamura, A. Gonsalves, S. Bulanov, M. Thévenet, C. Toth, J.-L. Vay *et al.*, Acceleration of high charge ion beams with achromatic divergence by petawatt laser pulses, Phys. Rev. Accel. Beams Beams, **23**, 021302 (2020).

[4] M. Fuchs, R. Weingartner, A. Popp, Z. Major, S. Becker, J. Osterhoff, I. Cortrie, B. Zeitler, R. Hörlein, G. D. Tsakiris *et al.*, Laser-driven soft-x-ray undulator source, Nat. Phys. **5**, 826 (2009).

[5] A. Maksimchuk, S. Gu, K. Flippo, D. Umstadter, and V. Y. Bychenkov, Forward ion acceleration in thin films driven by a high-intensity laser, Phys. Rev. Lett. **84**, 4108 (2000).

[6] M. Borghesi, A. Mackinnon, D. H. Campbell, D. Hicks, S. Kar, P. K. Patel, D. Price, L. Romagnani, A. Schiavi, and O. Willi, Multi-MeV proton source investigations in ultra-intense laser-foil interactions, Phys. Rev. Lett. **92**, 055003 (2004).

[7] T. Cowan, J. Fuchs, H. Ruhl, A. Kemp, P. Audebert, M. Roth, R. Stephens, I. Barton, A. Blazevic, E. Brambrink *et al.*, Ultralow emittance, multi-MeV proton beams from a laser virtual-cathode plasma accelerator, Phys. Rev. Lett. **92**, 204801 (2004).

[8] M. Roth, M. Allen, P. Audebert, A. Blazevic, E. Brambrink, T. Cowan, J. Fuchs, J. Gauthier, M. Geißel, M. Hegelich *et al.*, The generation of high-quality, intense ion beams by ultra-intense lasers, Plasma Phys. Controlled Fusion **44**, B99 (2002).

[9] B. Dromey, M. Coughlan, L. Senje, M. Taylor, S. Kuschel, B. Villagomez-Bernabe, R. Stefanuik, G. Nersisyan, L. Stella, J. Kohanoff *et al.*, Picosecond metrology of laser-driven proton bursts, Nat. Commun. **7**, 10642 (2016).

[10] S. V. Bulanov, J. J. Wilkens, T. Z. Esirkepov, G. Korn, G. Kraft, S. D. Kraft, M. Molls, and V. S. Khoroshkov, Laser ion acceleration for hadron therapy, Phys. Usp. **57**, 1149 (2014).

[11] J. Bin, L. Obst-Huebl, J.-H. Mao, K. Nakamura, L. D. Geulig, H. Chang, Q. Ji, L. He, J. De Chant, Z. Kober *et al.*, A new platform for ultra-high dose rate radiobiological research using the BELLA PW laser proton beamline, Sci. Rep. **12**, 1484 (2022).

[12] Y. Gao, R. Liu, C.-W. Chang, S. Charyyev, J. Zhou, J. D. Bradley, T. Liu, and X. Yang, A potential revolution in cancer treatment: A topical review of flash radiotherapy, J. Appl. Clin. Med. Phys. **23**, e13790 (2022).

[13] G. Yang, C. Lu, Z. Mei, X. Sun, J. Han, J. Qian, Y. Liang, Z. Pan, D. Kong, S. Xu *et al.*, Association of cancer stem cell radio-resistance under ultra-high dose rate flash irradiation with lysosome-mediated autophagy, Front. Cell Dev. Biol. **9**, 672693 (2021).

[14] M. Barberio, M. Scisciò, S. Vallières, F. Cardelli, N. Chen, S, G. Famulari, T. Gangolf, G. Revet, A. Schiavi, M. Senzacqua, and P. Antici, Laser-accelerated particle beams for stress testing of materials, Nat. Commun. **9**, 372 (2018).

[15] M. Barberio, M. Scisciò, S. Vallières, S. Veltri, A. Morabito, and P. Antici, Laser-generated proton beams for high-precision ultra-fast crystal synthesis, Sci. Rep. **7**, 12522 (2017).

[16] P. Patel, A. Mackinnon, M. Key, T. Cowan, M. Foord, M. Allen, D. Price, H. Ruhl, P. Springer, and R. Stephens, Isochoric heating of solid-density matter with an ultrafast proton beam, Phys. Rev. Lett. **91**, 125004 (2003).

[17] A. Y. Faenov, T. Pikuz, Y. Fukuda, M. Kando, H. Kotaki, T. Homma, K. Kawase, T. Kameshima, A. Pirozhkov, A. Yogo *et al.*, Submicron ionography of nanostructures using

a femtosecond-laser-driven-cluster-based source, Appl. Phys. Lett. **95**, 101107 (2009).

[18] M. Roth, T. Cowan, M. Key, S. Hatchett, C. Brown, W. Fountain, J. Johnson, D. Pennington, R. Snavely, S. Wilks *et al.*, Fast ignition by intense laser-accelerated proton beams, Phys. Rev. Lett. **86**, 436 (2001).

[19] R. Pompili, M. Anania, E. Chiadroni, A. Cianchi, M. Ferrario, V. Lollo, A. Notargiacomo, L. Picardi, C. Ronsivalle, J. Rosenzweig *et al.*, Compact and tunable focusing device for plasma wakefield acceleration, Rev. Sci. Instrum. **89**, 033302 (2018).

[20] M. Schollmeier, S. Becker, M. Geißel, K. Flippo, A. Blažević, S. Gaillard, D. Gautier, F. Grüner, K. Harres, M. Kimmel *et al.*, Controlled transport and focusing of laser-accelerated protons with miniature magnetic devices, Phys. Rev. Lett. **101**, 055004 (2008).

[21] M. Nishiuchi, I. Daito, M. Ikegami, H. Daido, M. Mori, S. Orimo, K. Ogura, A. Sagisaka, A. Yogo, A. Pirozhkov *et al.*, Focusing and spectral enhancement of a repetition-rated, laser-driven, divergent multi-MeV proton beam using permanent quadrupole magnets, Appl. Phys. Lett. **94**, 061107 (2009).

[22] M. Scisciò, M. Migliorati, L. Palumbo, and P. Antici, Design and optimization of a compact laser-driven proton beamline, Sci. Rep. **8**, 6299 (2018).

[23] J. Zhu, M. Wu, Q. Liao, Y. Geng, K. Zhu, C. Li, X. Xu, D. Li, Y. Shou, T. Yang *et al.*, Experimental demonstration of a laser proton accelerator with accurate beam control through image-relaying transport, Phys. Rev. Accel. Beams, **22**, 061302 (2019).

[24] I. Hofmann, Performance of solenoids versus quadrupoles in focusing and energy selection of laser accelerated protons, Phys. Rev. ST Accel. Beams **16**, 041302 (2013).

[25] T. Burris-Mog, K. Harres, F. Nürnberg, S. Busold, M. Bussmann, O. Deppert, G. Hoffmeister, M. Joost, M. Sobiella, A. Tauschwitz *et al.*, Laser accelerated protons captured and transported by a pulse power solenoid, Phys. Rev. ST Accel. Beams **14**, 121301 (2011).

[26] S. Busold, D. Schumacher, C. Brabetz, D. Jahn, F. Kroll, O. Deppert, U. Schramm, T. E. Cowan, A. Blažević, V. Bagnoud *et al.*, Towards highest peak intensities for ultra-short MeV-range ion bunches, Sci. Rep. **5**, 12459 (2015).

[27] F. Romano, F. Schillaci, G. Cirrone, G. Cuttone, V. Scuderi, L. Allegra, A. Amato, A. Amico, G. Candiano, G. De Luca *et al.*, The elimed transport and dosimetry beamline for laser-driven ion beams, Nucl. Instrum. Methods Phys. Res., Sect. A **829**, 153 (2016).

[28] F. Schillaci, G. Cirrone, G. Cuttone, M. Maggiore, L. Andó, A. Amato, M. Costa, G. Gallo, G. Korn, G. Larosa *et al.*, Design of the ELIMAIA ion collection system, J. Instrum. **10**, T12001 (2015).

[29] F.-E. Brack, F. Kroll, L. Gaus, C. Bernert, E. Beyreuther, T. E. Cowan, L. Karsch, S. Kraft, L. A. Kunz-Schughart, E. Lessmann *et al.*, Spectral and spatial shaping of laser-driven proton beams using a pulsed high-field magnet beamline, Sci. Rep. **10**, 9118 (2020).

[30] F. Kroll, F.-E. Brack, C. Bernert, S. Bock, E. Bodenstein, K. Brüchner, T. E. Cowan, L. Gaus, R. Gebhardt, U. Helbig *et al.*, Tumour irradiation in mice with a laser-accelerated proton beam, Nat. Phys. **18**, 316 (2022).

[31] K. Wang, K. Zhu, M. J. Easton, Y. Li, C. Lin, and X. Yan, Achromatic beamline design for a laser-driven proton therapy accelerator, Phys. Rev. Accel. Beams **23**, 111302 (2020).

[32] J. Zhu, M. Wu, K. Zhu, Y. Geng, Q. Liao, D. Li, T. Yang, M. Easton, C. Li, X. Xu *et al.*, Demonstration of tailored energy deposition in a laser proton accelerator, Phys. Rev. Accel. Beams Beams, **23**, 121304 (2020).

[33] M. Wu, J. Zhu, D. Li, T. Yang, Q. Liao, Y. Geng, X. Xu, C. Li, Y. Shou, Y. Zhao *et al.*, Collection and focusing of laser accelerated proton beam by an electromagnetic quadrupole triplet lens, Nucl. Instrum. Methods Phys. Res., Sect. A **955**, 163249 (2020).

[34] Y. Yan, T. Yang, D. Li, H. Cheng, Y. Li, M. Wu, Y. Fang, F. Li, Z. Guo, Z. Yuan *et al.*, Design of beam collection system with high transmission efficiency and tunablity, J. Phys. Conf. Ser. **2420**, 012111 (2023).

[35] X. Xu, Q. Liao, M. Wu, Y. Geng, D. Li, J. Zhu, C. Li, R. Hu, Y. Shou, Y. Chen *et al.*, Detection and analysis of laser driven proton beams by calibrated Gafchromic HD-V2 and MD-V3 radiochromic films, Rev. Sci. Instrum. **90**, 033306 (2019).

[36] James F. Ziegler, M. D. Ziegler, J. P. Biersack, SRIM–The stopping and range of ions in matter (2010), Nucl. Instrum. Methods Phys. Res., Sect. B **268**, 1818 (2010).

[37] F. Wagner, S. Bedacht, V. Bagnoud, O. Deppert, S. Geschwind, R. Jaeger, A. Ortner, A. Tebartz, B. Zielbauer, D. Hoffmann *et al.*, Simultaneous observation of angularly separated laser-driven proton beams accelerated via two different mechanisms, Phys. Plasmas, **22**, 063110 (2015).

[38] D. Zhou, D. Li, Y. Chen, M. Wu, T. Yang, H. Cheng, Y. Li, Y. Chen, Y. Li, Y. Geng *et al.*, Preparation of graphene on SiC by laser-accelerated pulsed ion beams, Chin. Phys. B **30**, 116106 (2021).

[39] D. Carroll, P. McKenna, O. Lundh, F. Lindau, C.-G. Wahlström, S. Bandyopadhyay, D. Pepler, D. Neely, S. Kar, P. Simpson *et al.*, Active manipulation of the spatial energy distribution of laser-accelerated proton beams, Phys. Rev. E **76**, 065401 (2007).

[40] F. Nürnberg, M. Schollmeier, E. Brambrink, A. Blažević, D. Carroll, K. Flippo, D. Gautier, M. Geißel, K. Harres, B. Hegelich *et al.*, Radiochromic film imaging spectroscopy of laser-accelerated proton beams, Rev. Sci. Instrum. **80**, 033301 (2009).

[41] Z. Zhao, B. Qin, X. Liu, W. Chen, and Q. Chen, Influence of fringing field and second-order aberrations on proton therapy gantry beamline, Nucl. Instrum. Methods Phys. Res., Sect. A **940**, 479 (2019).

[42] F. Schillaci, M. Maggiore, D. Rifuggiato, G. Cirrone, G. Cuttone, and D. Giove, Errors and optics study of a permanent magnet quadrupole system, J. Instrum. **10**, T05001 (2015).

[43] M. Wu, D. Li, J. Zhu, T. Yang, X. Hu, Y. Geng, K. Zhu, M. Easton, Y. Zhao, A. Zhang *et al.*, Emittance measurement along transport beam line for laser driven protons, Phys. Rev. Accel. Beams **23**, 031302 (2020).

[44] F. Li, Y. Wu, Z. Nie, B. Guo, X. Zhang, S. Huang, J. Zhang, Z. Cheng, Y. Ma, Y. Fang *et al.*, On the feasibility of sub-100 nm rad emittance measurement in plasma accelerators using permanent magnetic quadrupoles, Plasma Phys. Controlled Fusion **60**, 014029 (2017).

[45] Y.-X. Geng, Y.-R. Shou, J.-G. Zhu, X.-H. Xu, M.-J. Wu, P.-J. Wang, D.-Y. Li, R.-H. Hu, D.-H. Wang, Y.-Y. Zhao *et al.*, Generating proton beams exceeding 10 MeV using high contrast 60 TW laser, Chin. Phys. Lett. **35**, 092901 (2018).